

Experimental Validation of Multi-fidelity Models for Prognostics of Electromechanical Actuators

*Original*

Experimental Validation of Multi-fidelity Models for Prognostics of Electromechanical Actuators / Baldo, Leonardo; Berri, Pier Carlo; Dalla Vedova, Matteo; Maggiore, Paolo. - ELETTRONICO. - 7:(2022), pp. 32-42. ( European Conference of the PHM Society 2022 Turin, Italy July 6 thJuly 8 th , 2022) [10.36001/phme.2022.v7i1.3347].

*Availability:*

This version is available at: 11583/2991523 since: 2024-08-06T08:05:53Z

*Publisher:*

The Prognostics and Health Management Society

*Published*

DOI:10.36001/phme.2022.v7i1.3347

*Terms of use:*

This article is made available under terms and conditions as specified in the corresponding bibliographic description in the repository

*Publisher copyright*

(Article begins on next page)

# Experimental Validation of Multi-fidelity Models for Prognostics of Electromechanical Actuators

Leonardo Baldo<sup>1</sup>, Pier Carlo Berri<sup>1</sup>, Matteo D. L. Dalla Vedova<sup>1</sup>, and Paolo Maggiore<sup>1</sup>

<sup>1</sup> *Department of Mechanical and Aerospace Engineering (DIMEAS), Politecnico di Torino, Turin, 10129, Italy*

*leonardo.baldo@polito.it*

*pier.berri@polito.it*

*matteo.dallavedova@polito.it*

*paolo.maggiore@polito.it*

## ABSTRACT

The growing adoption of electrical energy as a secondary form of onboard power leads to an increase of electromechanical actuators (EMAs) use in aerospace applications. Therefore, innovative prognostic and diagnostic methodologies are becoming a fundamental tool to early identify faults propagation, prevent performance degradation, and ensure an acceptable level of safety and reliability of the system. Furthermore, prognostics entails further advantages, including a better ability to plan the maintenance of the various equipment, manage the warehouse and maintenance personnel, and a reduction in system management costs.

Frequently, such approaches require the development of typologies of numerical models capable of simulating the performance of the EMA with different levels of fidelity: monitoring models, suitably simplified to combine speed and accuracy with reduced computational costs, and high fidelity models (and high computational intensity), to generate databases, develop predictive algorithms and train machine learning surrogates. Because of this, the authors developed a high-fidelity multi-domain numerical model (HF) capable of accounting for a variety of physical phenomena and gradual failures in the EMA, as well as a low-fidelity counterpart (LF). This simplified model is derived by the HF and intended for monitoring applications. While maintaining a low computing cost, LF is fault sensitive and can simulate the system position, speed, and equivalent phase currents.

These models have been validated using a dedicated EMA test bench, designed and implemented by authors. The HF model can simulate the operation of the actuator in nominal conditions as well as in the presence of incipient mechanical faults, such as a variation in friction and an increase of backlash in the reduction gearbox.

Leonardo Baldo et al. This is an open-access article distributed under the terms of the Creative Commons Attribution 3.0 United States License, which permits unrestricted use, distribution, and reproduction in any medium, provided the original author and source are credited.

Comparing the preliminary results highlights satisfactory consistency between the experimental test bench and the two numerical models proposed by the authors.

## 1. INTRODUCTION

The adoption of the so-called "more electric" paradigm is slowly but steadily reshaping aircraft design and their operations, leading to the development of new technologies. At the same time, the buildup of complex and innovative solutions requires appropriate theoretical and modelling studies to gain the relevant knowledge base and scientific know-how concerning, among other aspects, their safety.

Moreover, More Electric Aircrafts (MEAs) embrace a completely new subsystems architecture (AbdElhafez & Forsyth, 2009), which gives birth to a brand-new set of requirements, aimed at reducing weight and fuel consumption by limiting the hydraulic and pneumatic subsystem influence on the overall aircraft.

A case in point is the development and adoption of Electromechanical Actuators (EMAs), whose deployment, which is in line with the new requirements linked to MEAs, requires a solid modelling back up.

In this sense, a general overview of EMAs solutions can be found in (Qiao et al., 2018) along with the related opportunities and challenges. EMAs are emerging as lighter and more efficient solutions (Garcia Garriga, Ponnusamy, & Mainini, 2018) than hydraulic actuators for flight controls. EMA use in aircraft is hence becoming more widespread but their extensive usage is still slowed down due to the limited experience in terms of safety and reliability, being the latter extremely important especially when EMAs are used as safety critical devices. Some problems are related to their critical modes, which are usually active (e.g. mechanical jamming of the transmission) and to EMC issues, whose prediction is challenging (Balaban et al., 2009) supplies a thorough review on typical critical EMA failure modes).

In other words, they lack the knowledge base which other actuator types have (e.g. hydraulic or hydrostatic ones), in relation to fault detection, identification (FDI), prognosis, reliability and safety in general. To support EMA usage, reliable prognostic tools are required to provide a precise estimation of the system actual state and to assess the Remaining Useful Life (RUL) of components and subsystems.

Therefore, a real time monitoring system based on intricate and highly tuned algorithms is crucial to guarantee and satisfy the expected safety standards (e.g. (Berri, Dalla Vedova, & Mainini, 2021)). On the other hand, Prognostics and Health Management (PHM) systems must rely on a detailed set of numerical models, which must be correctly tuned to reproduce the actuators' behaviour in terms of static and dynamic response (e.g. currents, voltages, speed, position etc).

This is the reason why a solid and detailed modelling study comes into place and becomes pivotal to allow a more capillary use of EMA in the aerospace sector ((Berri, Dalla Vedova, & Mainini, 2022)).

Thanks to the comparison between the real response of the operating components or systems (through a precise monitoring) and the nominal response, provided by a reference model, PHM methods can predict progressive failure evolution, thus estimating components RUL. In fact, according to acquired information, various decision making strategies (e.g. Sense-Infer-Plan-Act suggested in by (Mainini & Willcox, 2015)) can be used before the hidden failure could change into catastrophic or hazardous failure conditions. De facto, RUL estimation can be exploited to enhance mission readiness: aircraft operations can be rearranged dynamically, maintenance actions can be scheduled in more convenient ways and the entire integrated logistic support architecture can be improved (Sutharssan, Stoyanov, Bailey, & Yin, 2015). Finally, extensive usage of PHM methods on board could also result in a reduction of Life Cycle Costs (LCC) due to the high cut to maintenance costs (Williams, 2006).

It is now clear that models development and the relative tuning is a crucial step for a progressive and leading-edge design. However, models validation is just as important as their creation. The outputs, trends, values and the model predictions in general have to be thoroughly validated thanks to detailed and broad experimental data sets. Should not model predictions be validated, the results can not be considered credible and reliable at any point. Test benches, like the ones available in our laboratories, are ideal platforms to obtain and collect experience, know-how and data-sets which can then be used to experimentally validate pre-build models.

To all intents and purposes, models experimental validation is a largely widespread technique harnessed in all those engineering applications which involve the development of new simulation, monitoring and control models (e.g. (Di Rito, Denti, & Galatolo, 2008) and (Bertolino, De Martin, Jacazio, & Sorli, 2020)).

In particular, in this work, the authors have focused on the modelling and validation of backlash phenomena. They covered in depth the implementation of backlash simulation in the model as well as the related experimental set-up and tests. Backlash effects are very important in a mechanical transmission as neglecting them may cause the underestimation of critical aspects, for instance the overall stability (with limit cycles) and accuracy of the system (Maré, 2017). EMA are slowly starting to earn important roles in aircrafts flight control systems (e.g. Boeing B787) and their increasing affirmation is a direct consequence several fast-growing fields of research, such as the ones involving test benches construction, PHM strategies, model development and their validation.

## 2. TEST BENCH DESCRIPTION

During the last years, a highly modular, compact and versatile test bench has been developed to validate numerical models and to support research activities (Figure 1). To all intents and purposes, it was built around a pre-built model, explained later on in the paper and more in details in (Berri, Dalla Vedova, & Maggiore, 2019), to provide an experimental platform which could have been able to validate it.

Some in depth layout configuration and design principles concerning the test bench are explained in details in (Berri, Dalla Vedova, & Maggiore, 2021) and (Berri, 2021). However a brief description is mandatory for reasons of clarity.

The test bench can be roughly split up into:

- Actuation Module (Light-blue block)
- Transmission Module (Green block)
- Friction Load Simulation Module (Orange block)

Despite the industrial origin of many parts, their working principles are the same of aerospace components, thus the results are still valid. Conceivable differences are taken into account in the model when possible (e.g. power density). In other cases, they are not relevant for the dynamical behaviour (e.g. redundancies) and, as such, not modelled at all. The components expected behaviour in performed test is therefore assumed to be faithful enough with respect to aerospace hardware for the validation of the models (Berri, 2021) (Giangrande et al., 2018).

### 2.1. Actuation Module

The actuation module is made up of an integrated Siemens motor environment, the *SI20 AC/AC Trainer Package*. This package provides full authority for the shaft motion thanks to proprietary software, inverters and control units. Through a PC (1) and the Control Unit (2), the required command is generated and then sent to the motor (3). The motor output shaft is linked to a gearbox (4) input shaft through an elastic coupling. The test bench architecture emulates an actual typical EMA implementation, with a high gear-ratio mechanical gearbox placed at the motor output shaft.

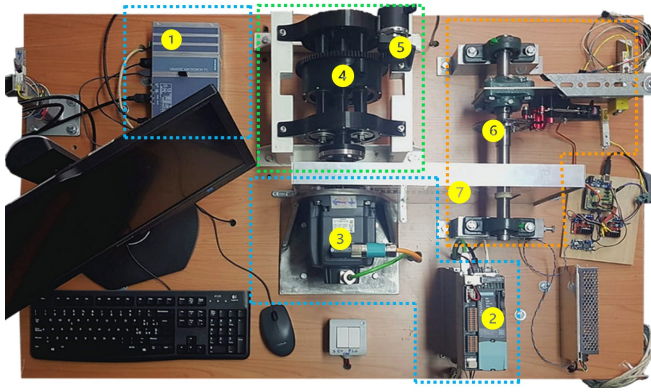


Figure 1. The test bench.

The implemented motor is a Siemens three phase, Permanent Magnet Synchronous Motor (PMSM): the S 1FK7060-2AC71-1CA0. This motor is controlled by a Siemens inverter which also logs motor electrical parameters with a frequency of  $400Hz$ . Table 1 shows the motor main engineering characteristics (where the notes  $60K$  and  $100K$  refer to an over-temperature of  $60K$  and  $100$  respectively).

### 2.2. Transmission Module: the Planetary Gearbox

As stated before, the test bench involves a planetary gearbox to be consistent with real life EMAs applications.

In fact, in EMAs classic configurations, a gearbox is an essential assembly component ((Qiao et al., 2018), (De Martin, Jacazio, & Vachtsevanos, 2017), (Maré, 2017)): usually, the user requires high torques and relatively low angular speeds. On the other hand, high torque motor are generally cumbersome and heavy, consequently they are not a viable solution where lightness and compactness is an essential requirement. The solution is exploiting a smaller motor with lower available torque but higher maximum angular speed and then, through a gearbox, reducing angular speeds while increasing torque. It goes without saying that, being gearboxes essential components, they must be considered inside the diagnostic and prognostic model loops.

The high transmission ratio (1 : 124) gearbox has been en-

tirely designed, built and assembled inside our laboratories starting from a Wolfrom drive layout (Garcia et al., 2019). Through the careful tuning of Wolfrom drive design parameters, a lightweight, high efficiency, additive manufacturing based planetary gearbox had been obtained and explained in (Berri, Dalla Vedova, Maggiore, & Riva, June 2020). Figure 2 shows the gearbox rendering.

The motion is picked up by an external incremental encoder (5) (5000 pulses per revolution), which is mounted on a carefully designed encoder support, engaging with the external output ring of the gearbox thanks to a spur gear.

The encoder support provides variable mechanical play between the encoder and the external output ring of the transmission, thanks to a micrometer. In this way, backlash effect can be reproduced by varying the mechanical play and useful data can be saved. Hence, backlash is introduced in the test bench downstream of the gearbox, between the user output gear and the encoder.

The encoder support assembly is composed of two FDM built pieces and a micrometer as seen in the rendering in figure 3 (Baldo, 2021).

### 2.3. Friction Load simulation module

A friction module (Figure 4) is essential to simulate realistic conditions, for instance the presence of progressive failures or variable friction due to components wear-out.

This is achieved through a braking torque obtained with a disk brake system, controlled in closed loop with a force sensor. In fact, another steel shaft (6) is placed parallel to the gearbox and fixed to the test bench structure with two self-aligning bearing assemblies. A chain (7) (enclosed in a safety case) links the motor output shaft with the braking shaft through a sprocket and the steel disk is fixed to the braking shaft.

The brake is actuated via a simple servomotor, similar to the ones used in the model making sector. It has to be noted that, the friction block acts directly on the motor output shaft and not on the overall gearbox output. This is an arbitrary and conscious choice in order not to excessively stress the planetary gearbox (PLA based), hence strictly linked to the test bench structural characteristics.

Table 1. Test bench motor main characteristics.

Characteristic	Value
Rated speed (100 K)	2000 rpm
Number of poles	8
Rated torque (100 K)	5.3 Nm
Rated current	3.0 A
Static torque (60 K)	5.00 Nm
Static torque (100 K)	6.0 Nm
Stall current (60 K)	2.55 A
Stall current (100 K)	3.15 A
Moment of inertia	7.700 kgcm <sup>2</sup>
Efficiency	90.00

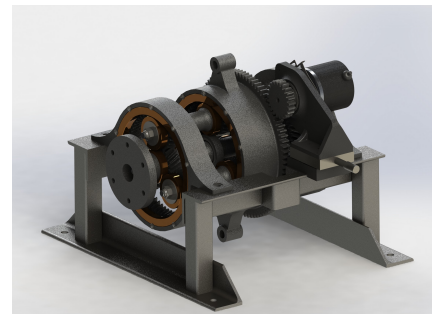


Figure 2. Gearbox rendering.

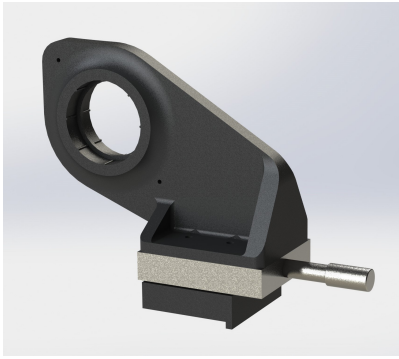


Figure 3. Encoder support assembly rendering.

The brake can generate around  $20 - 30 Nm$  of torque; on the other hand the stall torque of the Siemens motor is around  $6 Nm$ . This would have led to the servomotor working well outside its optimal operating range with increased internal frictions, random errors, lower test repeatability etc. Thanks to the chain transmission ratio, the braking torque felt by the driving shaft (i.e. motor shaft) is lower, therefore the servomotor can work in the best conditions possible.

The servomotor output shaft is connected with a steel rod to the brake assembly, consisting of two pads which can make contact with the disk, generating friction, hence transferring an external load to the motor thanks to the steel chain. A load cell is mounted to the metal plate to measure the mechanical deformation during the tests.

The control is handled via a PI controller, which stands for "Proportional-Integral". This special category of controllers, widely used in industrial applications, employs a simple proportional logic with a constant gain and an integral action aimed at reducing the steady state error. A derivative controller is not used since in this application the error reduction at steady state is much more important than response.

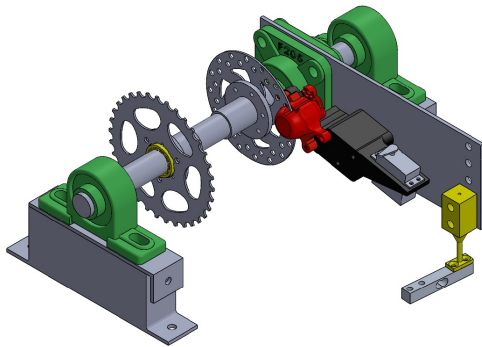


Figure 4. Braking module.

### 3. THE MODEL

#### 3.1. Model Description

For the sake of clarity, a brief description of the implemented EMA model is here reported, even though an in depth explanation can be found in (Berri, 2021). Moreover, a detailed description of the proposed models as well as the the explanation of the proper purposes, objectives and limitation is reported in (Berri, 2021), (Berri et al., 2019) and (Berri et al., 2018).

The EMA model block diagram is presented in Figure 5 and it shows the main interactions between the Simulink sub models, as well as the model's inputs and outputs.

It has to be recalled that this model is further integrated into an higher level Simulink model, which takes into account the signal acquisition and filtering process, the command module, the load signal etc.

The model has been realised thanks to a physical-based approach: actual equations, which describe system physical phenomena, are implemented in Simulink blocks (e.g. EM motor equations, dynamic equations etc). Required data for the models have been taken from components data sheets or obtained thanks to experimental tests. More details on the underlying equations and data can be found in (Berri, 2021), (Sciandra, 2020) and (Boschetti, 2020).

The *set* signal is inherited from the command module, from which it is possible to generate different command shapes (e.g. ramp, step, chirp, sinusoidal) and select their main parameters. The *Flight Condition* signal is provided from a "Repeating sequence" block that provides the model with the load value at the required time (linear interpolation is used if load cell values do not have the same sample time as the HF model). The raw data are supplied from the external load cell to simulate the external torque, with a Matlab script and an Arduino Board as a low level electronic interface.

#### 3.1.1. Actuator Control Electronics (ACE)

The Actuator Control Electronics model takes as inputs the *set* signal (position or speed) as well as the motor measured speed and user position and it is responsible for the generation of the requested torque and current.

In other words, it carries out the computation of the control law according to the selected command. This block enforces a PID controller with a low pass derivative filter, current saturation and anti-windup protection. The choice of implementing a PID controller is backed up by the enormous number of industrial applications which are based on this control strategy: this kind of controller is still the industry standard and that is the reason why it is implemented in this model. A white band noise signal is added to simulate electromagnetic noise on the command line. The output of the module is the stator current, obtained by dividing the torque (inherited from the PID controller) by the back-EMF coefficient of the motor.

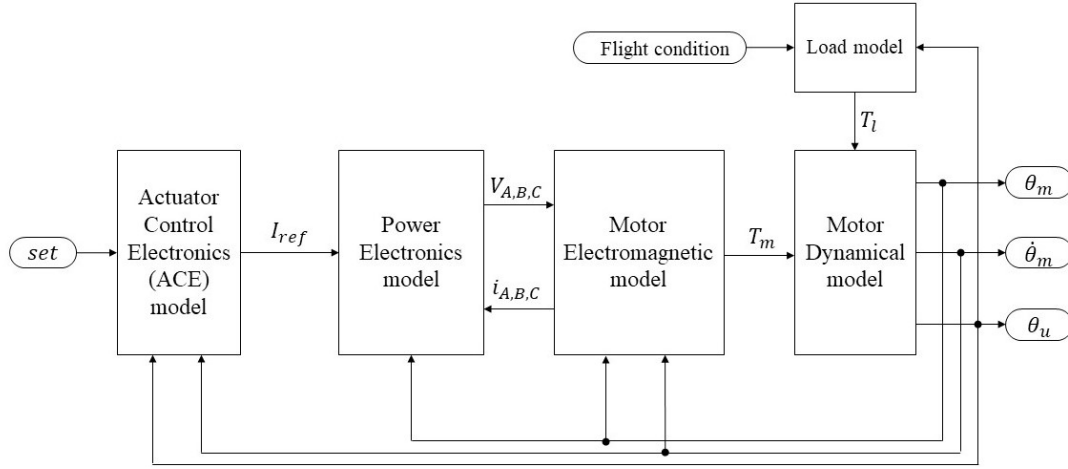


Figure 5. EMA functional block diagram as taken from (Berri,2021).

### 3.1.2. Power Electronics Model (PEM)

The PEM is made up of three main subsystems, each one with its separated functions:

- The first one is responsible for the evolution of the phase currents (i.e. the commutation sequence of the phases). Inverted Clarke-Park inverse transformation (with multiple reference systems) are exploited.  $I_{ref}$  is split into the three phase currents thanks to the information given from the angular position of the motor; hence the three motor phases are switched on or off, thanks to the commutation logic.
- The second module carries out the hysteresis control, comparing the stator phase currents with the respective reference currents. These currents then control the activation of the three phases' MOSFETs. If the difference between a phase current and the reference current lies outside a hysteresis band, the corresponding phase will be powered; otherwise, it will be switched off. As a matter of fact, this block generates a high frequency square wave which can be intended as a PWM signal.
- The last block consists of a Three-phase bridge, implemented via Simscape and made up of six MOSFETs with protection diodes. This block takes as input three Boolean values generated from the previous module. Extreme caution was placed in order not to create short circuit situations.

### 3.1.3. Motor Electromagnetic Model

The Electromagnetic model is responsible for the computation of the Back-EMF coefficient, of the currents flowing in the three phases and the calculation of the motor torque. The currents are dynamically estimated thanks to three star connected RL branches (with floating neutral) which model the

three stator phases (in Simscape). Knowing both the currents and the back-EMF coefficient at each integration step and with the assumption of linear superposition of each phase contribution, the total motor torque is easily obtainable (Eq. 1):

$$T_m = \sum_{j=A,B,C} i_j \cdot k_j \quad (1)$$

with  $i_j$  the current and  $k_j$  the back-EMF coefficient on each one of the three phases  $A, B, C$ . Finally, a saturation is placed to model magnetic flux non linearity. The total thrust is then sent to the Dynamical Model.

### 3.1.4. Load Model

The load module is just a simple gain which takes into account the geometry of the test bench, thus computing a torque, starting from a force measurement. De facto, the gain is the distance (arm) between the force cell and the breaking shaft explained in Section 2.3.

### 3.1.5. Motor Dynamical Model: Backlash

The motor and transmission dynamical model serves as the core of the simulation; it takes as inputs the motor torque and the external torque and determines the motor and users positions.

It features a second order dynamical system (Eq. 2) and, through its multiple integration, the user angular position can be obtained.

$$T_m - T_l = J_m \frac{d^2\theta_m}{dt^2} + C_m \frac{d\theta_m}{dt} \quad (2)$$

where  $T_m$  is the motor torque,  $T_l$  is the external torque (Load),  $J_m$  is the assembly inertia,  $C_m$  is the viscous friction coef-

ficient of the assembly and  $\theta_m$  is the motor position. The dynamical model takes into account different non linearity:

- the effects of dry friction (implemented with the Borello model (Borello & Dalla Vedova, July 2006))
- the effects of viscous friction (with the viscous friction coefficient  $C_m$  dependent on speed)
- the effects of the assembly inertia (estimated with CAD tool)
- the effects of end-stops (detected with a saturated position integrator)
- backlash phenomena

Backlash phenomena are particularly important and, as such, they require a more in depth explanation.

Backlash is a mechanical non linearity which greatly impacts the goodness of speed and position control performance, in particular if high precision is required. It is caused by the mechanical play between parts, typically gears and causes irregularities in the transmission, since there are some moments where the gears are not touching each other and then they suddenly come into contact. Moreover, when the gap caused by the mechanical play is wide open, the output gear can not be controlled (Nordin & Gutman, 2002).

Even if usually electromechanical actuator parts are designed with a small interference, wear and degradation due to use may result in mechanical plays after some time.

Therefore, a detailed modelling of a mechanical actuator can not escape considering backlash into the control loop since excluding it may cause the underestimation of critical aspects, for instance the overall stability (with limit cycles) and accuracy of the system. As stated in (Maré, 2017), gear backlash is detrimental for the service life of the contacts and for control stability, especially when the actuators have to work in position control loops (as in primary and secondary flight control actuators).

Moreover, other negative effects of joint backlash can be detected in a mechanical transmission such as a deleterious impact on frequency response or different hazardous conditions (e.g. load oscillations leading to flight controls flutter phenomena or steerable landing gear shimmy) (Maré, 2017).

For the purpose of this model a very rough backlash modelling has been implemented thanks to a simulink block which (hysteresis band) placed on the user shaft position. The hysteresis band acts as reported in Eq. 3 (taken from (Berri, 2021)), with a band-width of  $2BLK$  from the motor position.

$$\theta_u(t) = \begin{cases} \frac{\theta_m(t)}{i} + BLK, & \text{if } \theta_u(t - dt) - \frac{\theta_m(t)}{i} \geq BLK \\ \frac{\theta_m(t)}{i} - BLK, & \text{if } \theta_u(t - dt) - \frac{\theta_m(t)}{i} \leq -BLK \\ \theta_u(t - dt), & \text{otherwise} \end{cases} \quad (3)$$

Where  $\theta_u$  is the user position  $t$  is the simulation time,  $dt$  is the step time,  $i$  is the gear ratio and  $BLK$  is the backlash amplitude. The "if" condition is determined by the difference between the user position at the simulation step (involving  $i$ ) and the user position at the simulation step before.

This simple backlash modelling solution presents some limitations. In fact, the model outputs acceptable predictions only if the primary backlash source is deemed to be between the output gear and the encoder gear. The reason is that, only in this condition, the inertia and load downstream of the mechanical play are negligible.

In the future, a more detailed and precise backlash modelling may be taken into account: for instance, a multi-body simulation of the overall transmission to highlight the multiple degrees of freedom of each part.

### 3.2. An Insight on the Low Fidelity Model

As already mentioned, a Low Fidelity model (LF) has been developed, starting from the High Fidelity model.

The LF presents a very similar structure compared with the HF model (5): the various blocks share the same high level functions but they are simplified and lightened.

The LF sees inside a command generator, a controller module, an electromagnetic model module as well as a load and a dynamical model. The only main difference with respect to the HF model lies in the exploitation of an equivalent single-phase approach. The equivalent single phase is strictly related to the quadrature component reconstructed from the measured current flowing in the stator windings. The calculation utilise Clarke-Park transformation and a low pass filter.

Furthermore, some minor simplifications in each block can be found, such as a lightened PID controller, without any anti-windup or derivative filtering system. Finally the mechanical model considers a linear contribution of viscous effects.

This model has been validated thanks to the already experimentally validated HF model in a multi parameter process. Given the strong system-oriented characteristics of the problem, the adopted tuning strategy and performance validation metric has taken into consideration various aspects aimed at making the LF model (integrated in the prognostic algorithm) capable of simulating the real system with the desired behaviour: low computational time, medium to high accuracy and sensibility, satisfactorily low error with respect to the HF model. A more in depth description of the model and the relative validation and tuning process can be found in (Berri, 2021), (Berri et al., 2019) and (Berri et al., 2018).

## 4. RESULTS

User speed and position measurements have been acquired thanks to the external encoder, whereas motor speed and position measurements have been obtained thanks to the Control Unit software, through a resolver sensor integrated in the motor.

#### 4.1. Low Fidelity and High fidelity

Figure 6 and 7 shows a very good behaviour of the LF model, which is able to simulate the commanded signal with minimum differences, despite the much lower computational cost and the much simpler modelling approach.

This confirms that a real-time monitoring system can be approached with low fidelity models trained with the help of more complex and computational intensive high fidelity ones. In particular, position and speed are almost identical. The LF result has been experimentally validated in nominal conditions and displays valid results.

#### 4.2. Non-nominal conditions.

The installation of the external encoder support assembly, combined with the backlash modelling, has allowed us to experimentally validate the HF model in the presence of incipient mechanical faults.

In fact, variable backlash has been inserted at the output ring of the planetary gearbox.

A minor tuning of model controller gains and parameters has been carried out, comparing the data with the information given by Siemens software (e.g. proportional gain, error position saturation, current saturation) and with CAD evaluation (i.e. the planetary gearbox moment of inertia).

A first set of measurements and calibration has been carried out:

- the horizontal measurement read from the micrometer ( $d$ ) (starting from  $14mm$ );
- the distance between the centers of the gears (Wheelbase distance  $MW$ );

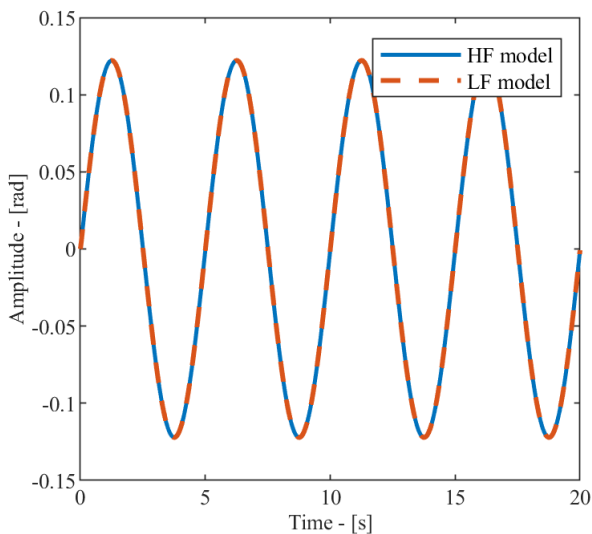


Figure 6. Comparison between LF and HF position predictions.

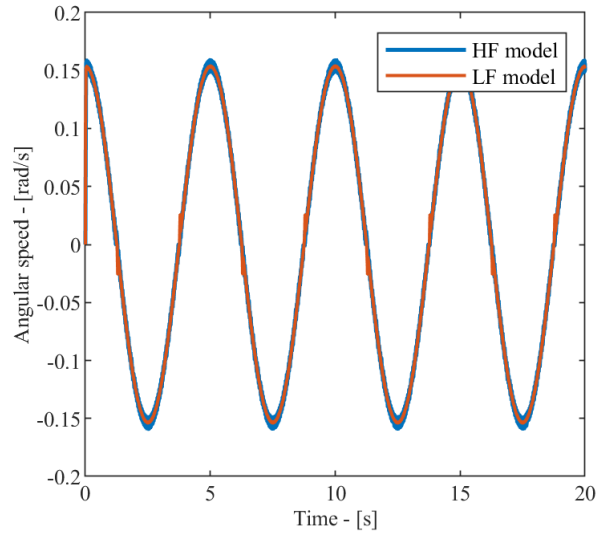


Figure 7. Comparison between LF and HF angular speed predictions.

- the radial spacing  $\Delta_{RS}$ , which is defined as the wheelbase difference with respect to the zero backlash condition:

$$\Delta_{RS} = MW - MW_{ZeroBacklash} \quad (4)$$

Then a theoretical Backlash formula (taken from (Boggio, 2021)) has been used to estimate backlash amplitude:

$$Est.BLK[^\circ] = \frac{\Delta_{RS} \cdot \tan \phi}{z} \cdot m \cdot \frac{180^\circ}{\pi} \quad (5)$$

which refers to ideal teeth profiles.  $\phi$  is the pressure angle (in this case  $20^\circ$ ),  $m$  is the gear module (in this case 2) and  $z$  is the number of teeth of the output ring of the planetary gearbox.

A set of measurement has been completed and shown in Table 2, comparing the actual backlash read from the encoder with the one estimated using Eq. 5.

It has to be noted that the gearbox assembly as a whole shows an intrinsic and uncontrollable backlash due to mounting, coupling and manufacturing tolerances; all these contributions sum up and are considered to be equal to  $0.3667^\circ$ .

This is shown in Table 2, with the sixth column which reports the "net" backlash, that is the measured backlash (column Exp. BLK) minus the intrinsic (nominal) backlash. Therefore, the last two columns can be compared to show the adherence of the results obtained with theoretical formula with the experimental values.

Figure 8 shows that the values are indeed very similar. They tend to be different at higher radial spacing values (that is

lower horizontal distances) due to the gears involute curve tooth profile which is not precise but approximated due to the FDM manufacturing process.

This preliminary analysis has been useful to foresee reasonable backlash parameters and to limit the backlash amplitude to a certain acceptable range so that the "geometrical" calculation and the experimental measurement do not diverge in an excessive way.

The test campaign has been carried out with a position command with the following characteristics:

- Sinusoidal waveform;
- Amplitude:  $7^\circ$ ;
- Bias:  $0^\circ$
- Frequency:  $0.2Hz$ .

Figure 9 shows good model behaviour in zero external backlash conditions (i.e. the first row of Table 2 with only nominal backlash). If we look at the highest point of the signal, it is possible to see the nominal backlash in action, both on the experimental signal and on the modelled one.

The amplitude of the experimental signal is slightly bigger than the modelled one. This can be traced back to minor imprecision inside the acquisition modules; the error has been proved to be constant as the gear backlash amplitude changes, hence minor tunings of internal gains will lessen the amplitude differences.

Comparisons between modelling and experimental results regarding no-load tests are shown in Figure 11 and Figure 10 where position and speed data are reported.

Three graphs are reported for position and speed as they refer to zero backlash condition (test no. 1 in Table 2), medium

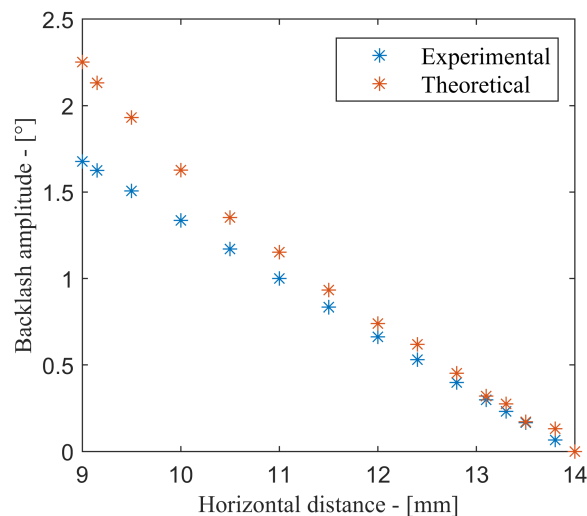


Figure 8. Comparison between theoretical and experimental backlash.

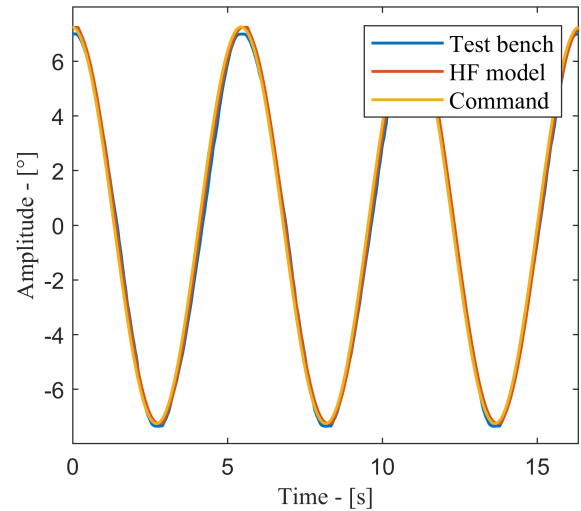


Figure 9. Commanded position, Simulink Model and Test Bench in zero backlash condition.

backlash condition (test no. 7 in Table 2) and maximum backlash condition between the gears (test no. 14 in Table 2). The graphs show promising results at steady states regimes, as the model is able to reproduce the intricate relationships between mechanical parts with a quite basic backlash modelling.

On the contrary, in transient states the model does not reproduce the effective trend efficiently, probably due to difficulties of modelling transient regimes, which are known to present multiple non linearities that have to be addressed separately. Hence this part is not shown.

Nonetheless, the model is able to distinguish between moments where the gears are in contact with each others and moments where there is no contact at all.

In addition, as can be noted in Figure 10 concerning speed comparisons, the model can successfully predict even small spikes, proving the goodness of the model design and confirming the validity of the overall model.

Position comparison shows excellent forecasting, especially at steady state, even in presence of maximum backlash conditions: at the highest and lowest value in the sinusoidal motion the model manages to deliver the typical horizontal line with the right time length.

In those conditions there is no contact between the gears. Therefore, even if the command is transferred to the motor and to the gearbox, the encoder gear still does not feel any movement. Only when the gap is closed, the motion is transmitted to the gear.

As reported in (Maré, 2017), this is one of backlash most detrimental effects, since there is a delay in the transmission and the user gear is free to move.

In the steeper part of the sinusoidal motion, the position is not influenced by backlash at all, since the gears always move in the same direction.

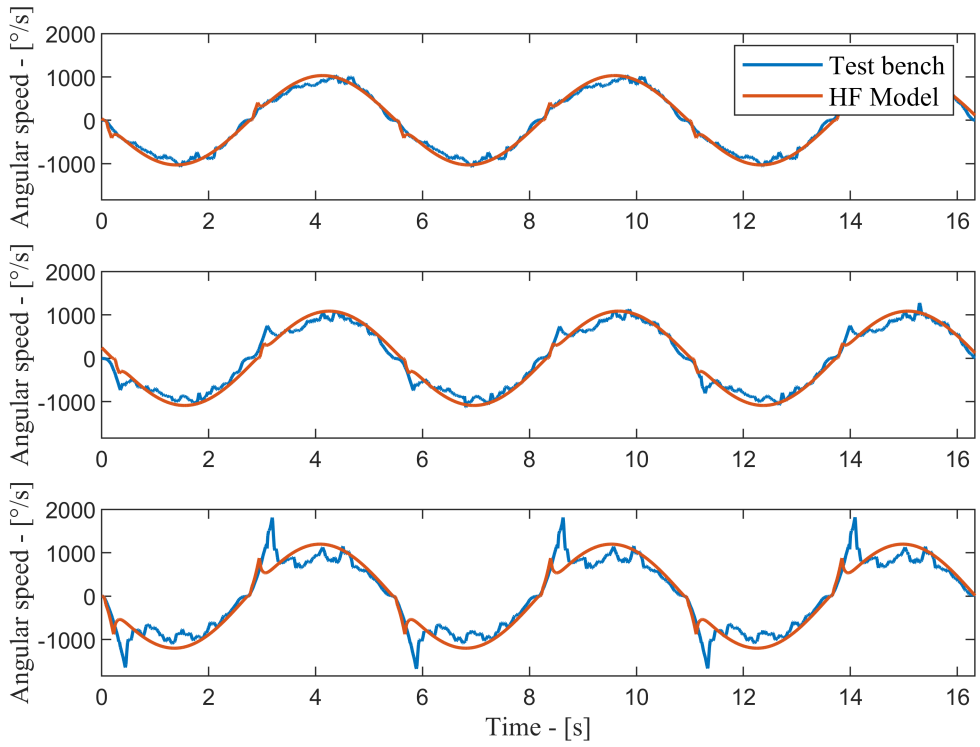


Figure 10. Model and experimental speed data in different backlash conditions (14mm – 12.4mm – 9.15mm).

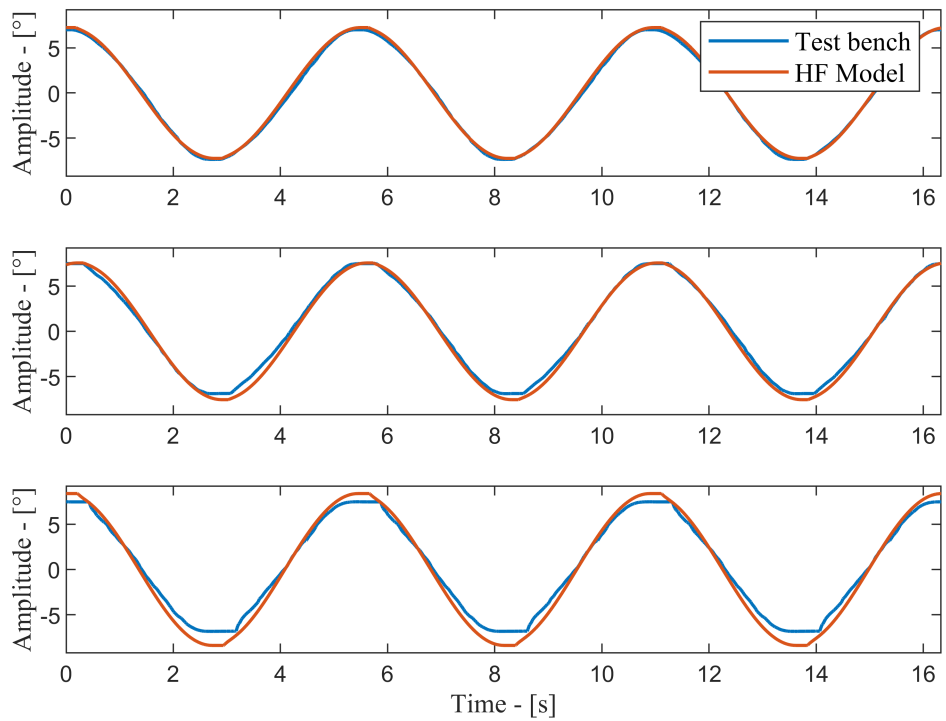


Figure 11. Model and experimental position data in different backlash conditions (14mm – 12.4mm – 9.15mm).

Table 2. Estimated and experimental backlash.

-	<b>d</b>	<b>MW</b>	$\Delta_{RS}$	<b>Exp. BLK</b>	<b>Net BLK</b>	<b>Est. BLK</b>
1	14	108.43	0	0.3667	0	0
2	13.8	108.57	0.14	0.4985	0.1318	0.0664
3	13.5	108.78	0.35	0.5386	0.1719	0.1653
...						
7	12.4	109.55	1.12	0.9855	0.6188	0.5308
8	12	109.83	1.4	1.1058	0.7391	0.6635
9	11.5	110.19	1.76	1.3006	0.9339	0.8342
...						
13	9.5	111.61	3.18	2.2976	1.9309	1.5072
14	9.15	111.86	3.43	2.4981	2.1314	1.6257
15	9	111.97	3.54	2.6184	2.2517	1.6778

## 5. CONCLUSION

A new numerical HF model, which is able to simulate successfully backlash conditions, has been developed by the authors and presented showing remarkable ability to foresee trends in position and speed change at steady-states regimes. In fact, the model has proved significant ability to simulate the complex contact dynamics between gears and to distinguish between contact and non-contact integration steps. Furthermore, even small spikes and minor disturbances are reproduced as well.

These trends and the model itself has been validated using an updated test bench designed and assembled by the authors. The newly developed model can be further modified and improved involving more accurate backlash modelling which might be able to track even transient regimes of speed and position.

Moreover, a parallel low fidelity model has been refined. The comparison between the two models shows a good trend overlap, highlighting the quality of the LF model.

Finally, additional validation and comparisons will be carried out with variable friction, exploiting the load module on the test bench: this will further verify the model goodness in presence of strong non linearities. Real-life applications for this model are endless, especially if applied on Low Fidelity models which could run in real-time. The real implementation of these techniques is deemed to be cost-effective, as the computational burden is reduced and necessary components (e.g. sensors) and technologies are already largely widespread in the aerospace sector.

## ACKNOWLEDGMENT

The authors wish to thank Matteo Bertone and Luca Boggio for the work carried out during their master theses.

## NOMENCLATURE

$I_{ref}$	Reference current value
$i_j$	Actual current in the $j$ -th phase
$k_j$	Back-EMF coefficient for the $j$ -th phase
$T_m$	Motor torque
$T_l$	External torque (load)
$J_m$	Actuator's rotating assembly inertia
$C_m$	Actuator's rotating assembly viscous friction coefficient
$\theta_m$	Motor mechanical position (gearbox upstream input)
$BLK$	Backlash amplitude
$\theta_u$	User position (gearbox downstream output)
$t$	Simulation time
$dt$	Simulation step time
$MW$	Wheelbase distance
$d$	Horizontal measurement read from the micrometer
$\Delta_{rs}$	Radial spacing
$Est.BLK$	Estimated theoretical backlash amplitude
$\phi$	Pressure angle
$m$	Gear module
$z$	Number of teeth
$Exp.BLK$	Experimental backlash amplitude
$Net.BLK$	Net backlash amplitude, without intrinsic backlash

## REFERENCES

- Abdelhafez, A., & Forsyth, A. (2009). A review of more-electric aircraft. In *International conference on aerospace sciences and aviation technology* (Vol. 13, pp. 1–13).
- Balaban, E., Bansal, P., Stoelting, P., Saxena, A., Goebel, K. F., & Curran, S. (2009). A diagnostic approach for electro-mechanical actuators in aerospace systems. In *2009 IEEE Aerospace Conference* (pp. 1–13).
- Baldo, L. (2021). Development of an experimental test bench for the validation of prognostic algorithms for electromechanical actuators. *MSc Thesis*.

- Berri, P. C. (2021). Design and development of algorithms and technologies applied to prognostics of aerospace systems. <https://iris.polito.it/handle/11583/2927464>.
- Berri, P. C., Dalla Vedova, M. D., & Mainini, L. (2021). Computational framework for real-time diagnostics and prognostics of aircraft actuation systems. *Computers in Industry*, 132, 103523.
- Berri, P. C., Dalla Vedova, M. D., & Mainini, L. (2022). Learning for predictions: Real-time reliability assessment of aerospace systems. *AIAA Journal*, 60(2), 566–577.
- Berri, P. C., Dalla Vedova, M. D. L., Maggiore, P., & Riva, G. (June 2020). Design and development of a planetary gearbox for electromechanical actuator test bench through additive manufacturing. In *Actuators* (Vol. 9, pp. Issue 2, Article number 35. ISSN: 20760825 - DOI:10.3390/ACT902035 - Scopus: 2-s2.0-85085740653).
- Bertolino, A. C., De Martin, A., Jacazio, G., & Sorli, M. (2020). Towards a phm system for electro-mechanical flight control actuators. *I-RIM 2020*, 4.
- Boggio, L. (2021). Development of an experimental test bench for the validation of prognostic algorithms for electromechanical actuators. *MSc Thesis*.
- Borello, L., & Dalla Vedova, M. D. L. (July 2006). Load dependent coulomb friction: a mathematical and computational model for dynamic simulation in mechanical and aeronautical fields. *International Journal of Mechanics and Control (JoMaC)*, Vol. 7(No. 1), pp. 19–30.
- Boschetti, V. (2020). Development of an experimental test bench for the validation of prognostic algorithms for electromechanical actuators. *MSc Thesis*.
- De Martin, A., Jacazio, G., & Vachtsevanos, G. (2017). Windings fault detection and prognosis in electromechanical flight control actuators operating in active-active configuration. *International Journal of Prognostics and Health Management*, 8(2).
- Di Rito, G., Denti, E., & Galatolo, R. (2008). Development and experimental validation of real-time executable models of primary fly-by-wire actuators. *Proceedings of the Institution of Mechanical Engineers, Part I: Journal of Systems and Control Engineering*, 222(6), 523–542.
- Garcia, P. L., Crispel, S., Verstraten, T., Saerens, E., Vanderborght, B., & Lefeber, D. (2019). Wolfrom planetary gear trains for lightweight, human-centered robotics. In *International conference on gears 2019* (pp. 753–764).
- Garcia Garriga, A., Ponnusamy, S. S., & Mainini, L. (2018). A multi-fidelity framework to support the design of more-electric actuation. In *2018 multidisciplinary analysis and optimization conference* (p. 3741).
- Giangrande, P., Madonna, V., Sala, G., Kladas, A., Gerada, C., & Galea, M. (2018). Design and testing of pmsm for aerospace ema applications. In *Iecon 2018-44th annual conference of the ieee industrial electronics society* (pp. 2038–2043).
- Mainini, L., & Willcox, K. (2015). Surrogate modeling approach to support real-time structural assessment and decision making. *AIAA Journal*, 53(6), 1612–1626.
- Maré, J.-C. (2017). *Aerospace actuators 2: signal-by-wire and power-by-wire* (Vol. 2). John Wiley & Sons.
- Nordin, M., & Gutman, P.-O. (2002). Controlling mechanical systems with backlash—a survey. *Automatica*, 38(10), 1633–1649.
- Qiao, G., Liu, G., Shi, Z., Wang, Y., Ma, S., & Lim, T. C. (2018). A review of electromechanical actuators for more/all electric aircraft systems. *Proceedings of the Institution of Mechanical Engineers, Part C: Journal of Mechanical Engineering Science*, 232(22), 4128–4151.
- Sciandra, P. (2020). Development and experimental validation of prognostic algorithms for electromechanical actuators. *MSc Thesis*.
- Sutharssan, T., Stoyanov, S., Bailey, C., & Yin, C. (2015). Prognostic and health management for engineering systems: a review of the data-driven approach and algorithms. *The Journal of engineering*, 2015(7), 215–222.
- Williams, Z. (2006). Benefits of ivhm: an analytical approach. In *2006 ieee aerospace conference* (pp. 9–pp).